ADVANCED ENGINEERING MATERIALS
www.aem-journal.com

Ultra-Precision Processing of Conductive Materials via Electrorheological Fluid-Assisted Polishing

Yunwei Zhao, Xiaomin Liu, Yuhui Fang, and Changyong Cao**

Ultra-precision polishing of conductive components of novel electronic and optical devices at small scales is of paramount importance for achieving desired product performance and quality. Herein, the feasibility and performance of the electrorheological fluid-assisted polishing (ERFP) approach in processing conductive materials are theoretically and experimentally investigated. The combination models for ERFP fluid with various size ratios of the polarized particles are established and discussed. A theoretical model for calculating the material removal volume in the ERFP process is derived to predict the polishing performance and the surface profile of the specimens. The measured material removal profiles agree well with the theoretical predictions, confirming the effectiveness of the proposed model. Experimental results demonstrate that the removal volume decreases rapidly with the increasing gap size and the rotation speed. With a microneedle-like tool electrode, the ERFP is able to removal the material in a well-controlled way, demonstrating its ability to polish conductive materials with high resolution and accuracy.

The rapid development of image technology and optical network technology requires novel electronic and optical devices of small size and complex surfaces but well-controlled surface morphology and quality.[1] One representative example is the aspheric lens that has been widely used in digital image products due to its superior performance.[2] Currently, most aspheric lenses are manufactured by cemented carbide molds following a traditional process.[3] The molds should have accurate geometric dimensions and excellent surface smoothness. Therefore, a precision polishing process is essential to improve the surface quality of the mold. Traditionally, polishing pad and grinding head are used for the polishing work, with abrasive particles added between the workpiece and the polishing pad.[4] This approach will generate non-uniform contact forces on the workpiece surface due to the accumulation of abrasive particles, thereby affecting the efficiency and uniformity in the polishing process. In addition, the polishing wheel is not small enough for polishing mold of micro-scale sizes due to the limitation of machine tool and tool size. To overcome the drawbacks of the traditional contact polishing method with fixed abrasive particles, it is highly demand to explore new advanced polishing approaches that can continuously gather abrasive particles into the polishing area for a long time to achieve constant material removal rate.

Electrorheological (ER) fluid is a smart material that can be controlled to change the rheological property and viscosity reversibly under an external electric field.[5–9] The rheological behaviors can be easily altered with the application of an electric field and return to its original viscosity when the electric field is removed.[10] The ER fluid generally consists of two phases: solid particles with good dielectric properties as the dispersed phase and non-conducting liquids as the continuous phase.[11] The dispersed particles are usually inorganic materials that have high dielectric constants and strong polarization properties. However, the liquid continuous phase has a relatively lower permittivity and insulation properties. Without electric field, the dispersed particles are freely suspended in the continuous fluid phase, exhibiting properties similar with Newtonian fluids. After an electric field is applied, the dispersed solid particles will be polarized, thereby forming particle chains along the direction of the applied electric field and transforming into a Bingham fluid state.[12–14]

ER fluid has been explored for polishing processing of precision products. For example, Kaku et al. and Kuriyagawa et al. first mixed ultra-fine abrasives particles into the ER fluid to show almost the same rheological property as ER particles and applied the ER fluid with diamond, Al_2O_3, or SiC particles for optical microlenses.[2,15] Following that, extensive studies investigated the performance of electrorheological fluid-assisted polishing (ERFP), including the behavior of dispersed particles, machining principle, polishing tool, and processing parameters. The study on the behaviors of solid particles showed that the concentration of the abrasive particles increases with the applied voltage during rotation and becomes more effective for polishing small areas.

Dr. Y. Zhao, Dr. X. Liu
School of Mechanical Engineering
Beihua University
Jilin 132013, China
E-mail: xiaomin_liu@beihua.edu.cn

Y. Fang, Prof. C. Cao
Laboratory for Soft Machines and Electronics
School of Packaging
Michigan State University
East Lansing, MI 48824, USA
E-mail: ccao@msu.edu

Prof. C. Cao
Departments of Mechanical Engineering
Electrical and Computer Engineering
Michigan State University
East Lansing, MI 48824, USA

The ORCID identification number(s) for the author(s) of this article can be found under https://doi.org/10.1002/adem.202001109.

DOI: 10.1002/adem.202001109

The interaction force from the polarizable particles drives the abrasive particles to collide surfaces to remove materials. The relative larger forces acted on the abrasive particles are increasing with the applied electric field. The ERFP process can efficiently enhance machining rate by controlling the electric strength.[16] Simultaneously, a variety of polishing equipment and tools were used for different materials, such as microneedle-like tools for conductive materials, needle-ring tools for non-conductive materials, and wheel-like and integrated electrode tools for both materials. For example, Kuriyagawa et al.[15] used a microneedle-like tool of 3 mm diameter to finish small 3D parts, but smaller working gap is easy to produce discharge between tool electrode and workpiece. To overcome this problem, Zhang et al. presented two specially designed integrated tools using a parallel plate and a needle cylinder.[17,18] Akagami and Umehara also developed a multi-layered concentric electrode tool, assembled with copper rings as electrodes and polymer rings as electric isolators.[19] Su et al. utilized a wheel-like finishing tool made of copper to produce an excellent surface roughness of 1.04 nm after 25 min polishing.[20]

Material removal rate is one of the key factors for evaluating the ERFP process. It is strongly affected by a few parameters: the gap, speed, voltage, volume percentage, and material properties of the abrasive particles. These parameters can be used to analyze the physical process of material removal. In particular, the selection of gap size is determined by the target finishing effect. A slightly larger gap can generate high-quality and smooth surfaces, whereas smaller gap is more suitable for large amount of material removal. For example, Zhang et al. used a microgap of 50 μm to investigate the effective polishing region in which the abrasive particles of diamond were used as the conductive material.[21] Su et al. measured the removal depth with different applied voltage using a Zyko interferometer, revealing that the interaction forces between abrasive particles play a key role in the capability of material removal.[22] On the other hand, if the gap is fixed, the surface roughness proportionally increases with the speed and voltage; however, the volume percentage and the properties of abrasive particles have a complicated influence on lower concentration. The insufficient number of abrasive particles contributes to polishing; however, the abrasives particles are difficult to be attracted due to the reduction of ER effect in a high-concentration ER polishing slurry. Thus, the optimal volume percentage of abrasive particles depends on the type of ER fluid and the properties of abrasive particles. In general, ultra-fine diamond particles (e.g., Al_2O_3 or SiC particles) are used as abrasive materials to get sufficient surface roughness. In addition, some magnetic particles (e.g., Fe_3O_4 particles) are added to polish optical glass,[23] and the alumina abrasive particles are used to remove recast layer with many microcraters and cracks generated in the electrical discharge machining (EDM).[24]

In this study, we have theoretically and experimentally investigated the material removal capability of ERFP, including the influence of microstructure, maximum removal depth, and effective polishing area. A theoretical model for the material removal of ERFP for conductive materials is proposed based on a combination model of solid particles to analyze the interaction forces on the abrasive particles for material removal. The presented model is verified by experimental data using different gap sizes and rotation speeds. It is utilized to analyze the behaviors of material removal for tungsten carbide. The relationship between the material removal rate and the significant processing parameters is revealed and validated.

The SiC, Al_2O_3, and diamond particles that have high hardness can be added into the ER fluid to form an ERFP slurry. In general, starch particles are used as dispersed phase particles and are mixed with silicone oil at a specific percentage to form an ER fluid. Then, the abrasive particles are added to the ER fluid based on the actual polishing needs. The volume fraction, particle size, and type of the abrasive particles can be adjusted as necessary. The ER phenomena originates from polarization of dispersed phase particles under an electric field, which behavior can be observed by a high-resolution microscope (**Figure 1**a). When an electric field is applied, the microstructures of the polishing fluid changes and the ER particles are polarized to form particle chains along the direction of electric field. The particle chains will further aggregate together to form clusters of fiber chains, demonstrating a complicated microstructure of ERFP fluid (Figure 1b).

In this process, the abrasive particles show almost the same behaviors as ER particles, which connects the ER particles to form different microstructures (Figure 1c). The granularity of diamond particles is W1. When abrasive particles are very small (W1) compared with starch particles, the fine abrasive particles will attach on the surface of larger ER particles (Figure 1c(i)).When the SiC abrasive particles become larger (W5), individual abrasive particles are adsorbed between ER particles (Figure 1c(ii)). As shown in Figure 1c(iii), when SiC abrasive particles increase to the size of W10, the abrasive particles will be bounded in the particle chain by the ER particles. If the size of abrasive particles increases further (W20), the ER particles are attached on the ends of the abrasive particles (Figure 1c(iv)). However, when the diamond particles are W40, the ER particles will first gather together and then distribute at the two ends of the abrasive particles (Figure 1c(v)). Based on the observed microstructure of clustering polarized particles (Figure 1c) and the combination of carbonyl iron particles and silicon carbide abrasives in a magnetorheological abrasive flow finishing (MRAFF) process,[25] we assume that the solid particles are in a spherical shape for simplicity, and that the combination of ER particles with abrasive particles forms a unit cell of a body-centered tetragonal (BCT) structure (Figure 1d).

Due to the different size ratios of the solid particles, the abrasive particles will be attracted by ER particles in different ways. They may be adsorbed onto the particle chain, or wrapped in the particle chain to occupy the original locations of the ER particles, or bonded by ER particles to form particle chains. The size ratio of the solid particles is defined as $W_{\text{ratio}} = \frac{|d_{\text{ep}} - d_{\text{ap}}|}{d_{\text{ep}} + d_{\text{ap}}}$, where d_{ap} and d_{ep} are the diameters of abrasive particles and starch particles, respectively. We assume that the solid particles are in close contact with one another, and β is the angle between the central line of the bound particles and the chain particles and the direction of external electric field (Figure S1, Supporting Information). When β is less than 55°, the solid particles will attract each other; otherwise, these particles will repel each other. When $W_{\text{ratio}} \geq 0.57$, the granularity difference between particles is too large, and the particles of small size will preferentially gather on the surface of large particles, which make it difficult to form a BCT structure. When $0.14 \leq W_{\text{ratio}} < 0.57$, the particles of small

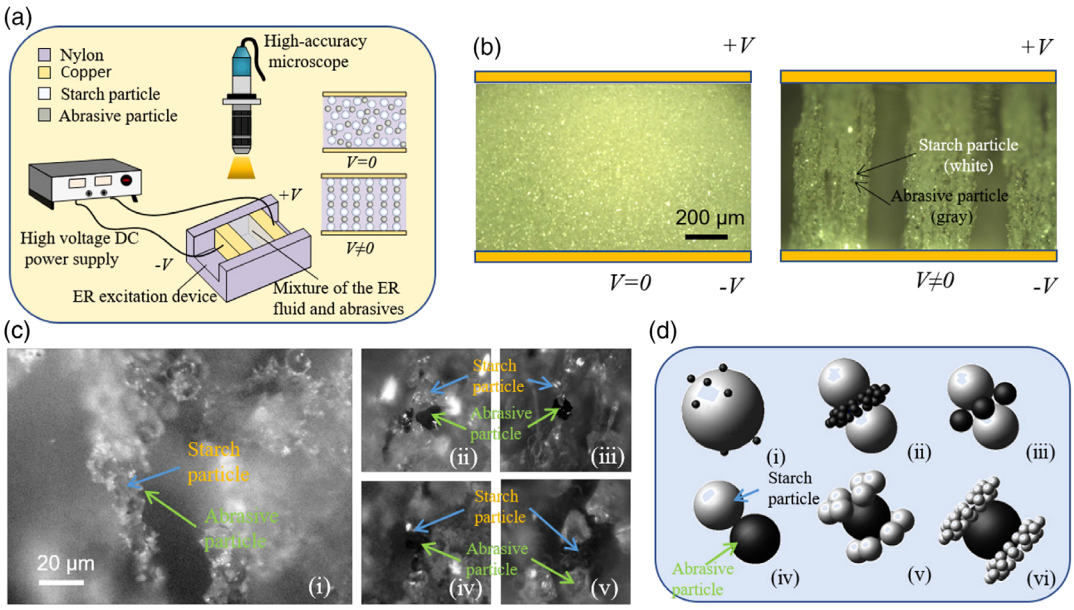

Figure 1. Microstructure and combination model of polarized particles in ERFP. a) Experimental setup for investigating the ER effect. The ER effect excitation device is made of a shell of insulating materials (Nylon), and two copper electrodes are placed in the channel to hold the ER mixture. The two copper electrodes are movable along the channel. b) Optical images of the microstructures of ER polishing slurry with SiC (W10, 10%) without and with voltage applied. c) Comparison of the microstructures of ER polishing slurries with different sizes of abrasive particles (W1–W40). The starch particle is W10. d) Combination models of the particles in the ER polishing solution when having different abrasive particle sizes.

size will first form particle clusters and then be absorbed between the large particles. At this time, β can be expressed as $\beta = \arccos(r_{ep} - r_{ap})/(r_{ep} + r_{ap})$. When $W_{ratio} < 0.14$, the particles of similar size can attract each other to form a single chain of particles or be absorbed between the chains of particles; then, β can be expressed as $\beta = \arccos r_{ep}/(r_{ep} + r_{ap})$.

Figure 1d(i,ii) shows the combination models of abrasive particles with the variable diameters of 0–3 μm. When abrasive particles are much smaller than ER particles, the small abrasive particles will attach on the surface of ER particles or form micromass between the ER particles. When the diameter increases to 4–14 μm, the abrasive particles will bond into the ER particle chains or insert into the ER particle chain to form a mixed chain-like structure (Figure 1d(iii,iv)). As the diameter of abrasive particles is larger than ER particles, ER particles will attach on the ends of abrasive particles. Figure 1d(v) shows the combined structure of the variable diameter abrasive particles within 15–37 μm. When the diameter of the abrasive particles is larger than 38 μm, the ER particles will aggregate into micromass due to their small size and then adhere to the ends of the abrasive particles (Figure 1d(vi)).

As shown in **Figure 2**a, the experimental setup for ERFP process is composed of the tool electrode, ER slurry, and the workpiece. The micropolishing tool electrode is made of copper, serving as positive electrode, whereas the conductor material workpiece works as a negative electrode. The slurry mixture made of fluid and abrasive particles for ER polishing is fed into the working gap between tool electrode and specimen surface. After an electric voltage is applied, the polishing slurry surrounding the tool electrode becomes stiffer and forms a tiny cylindrical bulge (Figure 2a). The polishing slurry rotates following the tool electrode; thereby, the abrasive particles in the slurry generate shearing effect to polish the surface of the workpiece.

The abrasive particles toughing the specimen surface, which is composed of half unit cells of the BCT structure, penetrate the workpiece surface due to the exerted normal forces. Taking the combination model with small abrasive particles and large ER particles (Figure 1d(iii)) as an example, the resultant normal force F_n applied on an abrasive particle that contacts the workpiece surface by the polarized ER particles in the same chain (Figure 2b,c) can be obtained by

$$F_n = F_{ep-ap} + F_{ap-ap} \tag{1}$$

where F_{ep-ap} is the resultant normal force exerted on the ith abrasive particle touching the specimen surface by the ER particles in the same chain, which can be calculated

$$\begin{aligned} F_{ep-ap} &= \sum_{i=1}^{n} \cos\theta_i F_{ij} \\ &= \sum_{i=1}^{n} \frac{3p_{epi}p_{apj}}{2\pi\varepsilon_0\varepsilon_f R_0^4} \cos\left(\arctan\left[\frac{R_0}{(2i-1)(r_{ep}+\delta/2)}\right]\right) \\ &\quad \times \sin^4\left(\arctan\left[\frac{R_0}{(2i-1)(r_{ep}+\delta/2)}\right]\right) \\ i &= 1, 2, \ldots\ldots n \end{aligned} \tag{2}$$

where ε_0 is the permittivity of free space, ε_f is the relative permittivity of dielectric fluid, R_0 is the distance from center of the abrasive particle to the axis of particle chain, r_{ep} is the radius of the ER particle, δ is the gap distance between two adjacent ER particles, and p_{epi} and p_{apj} are the dipole moment of ER particles

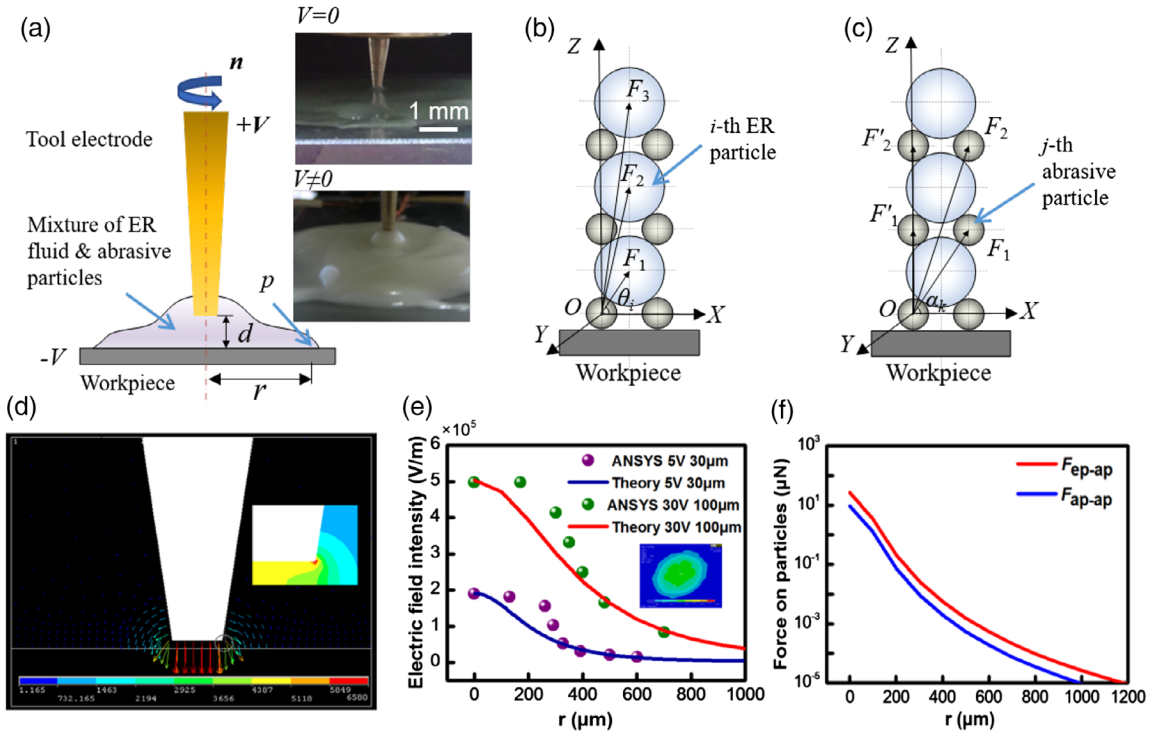

Figure 2. Working mechanism of ERFP process and the forces applied on the particles in a polishing slurry. a) Schematic illustration of the ERFP process for conductive materials. The inset images show the morphology of the mixture of ER fluid and abrasive particles without/with voltage applied. b) Schematic diagram of the attraction force F_{ep-ap} in ERFP. c) Schematic diagram of the attraction force F_{ap-ap}. d) numerical simulation results on the gradient electric field formed in the narrow working gap in ERFP process for conductive materials, in which the coefficient c_1 is 0.022 and the coefficient c_2 is 0.008. e) The variation of the electric field intensity within polishing region. f) The variation of the normal forces F_{ep-ap} and F_{ap-ap} in polishing region.

and that of abrasive particles, respectively. F_{ap-ap} is the resultant normal force exerted on the jth abrasive particle touching the specimen surface by other abrasive particles in different layers of the same chain, which can be calculated by

$$F_{ap-ap} = \sum_{l=1}^{n}\sum_{k=1}^{m} F_{jk}\cos\alpha_k = \sum_{l=1}^{n}\sum_{k=1}^{m} \frac{3p_{apj}p_{apk}}{2\pi\varepsilon_0\varepsilon_f(2r_{ep}+\delta)^4 l^4}\cos^5\left(\arctan\frac{2R_0\sin[(k-1)\pi/m]}{(2r_{ep}+\delta)l}\right)\ (l=1,2,\ldots n),\ (k=1,2,\ldots m) \quad (3)$$

where m is the number of abrasive particles distributed on the same layer, determined based on the size of the ER particle and that of the abrasive particle, and n is the number of layers in one single chain excluding the layer in which the considered jth abrasive particle stays.

Figure 2d shows the simulation results of the gradient electric field formed in the narrow working gap between the tool electrode and the specimen surface. As the voltage is applied, a strong electric field forms in the narrow working gap (50 μm), reaching a maximum field intensity of $6.5 \times 10^4\ \mathrm{V\,m^{-1}}$ under a small voltage of 2 V. The direction of electric field is perpendicular to specimen surface, and the maximum magnitude of the electric field establishes along tool electrode edge, where the maximal ER effect will be generated and abundant abrasive particles will be attracted to the region. The electric field can be described by $E = \frac{c_1 U s}{2\pi(c_2 r^2 + d^2)^{3/2}}$, where c_1 and c_2 are the coefficients, U is the applied voltage on the working gap, s is the area of the tool tip, d is the gap distance between the tool electrode and the workpiece surface, and r is the distance from point P on the workpiece to the center line of the tool (Figure 2a). Figure 2e presents the variation of the electric field intensity with the radius of r. It can be seen that the theoretical results agree very well with the numerical results from ANSYS in the range of the electrode diameter, indicating that the theoretical model is applicable to estimate the distribution of electric field intensity within the polishing region in ERFP. The relatively larger discrepancy at the radius range of 100–300 μm is mainly because the needle electrode is simplified to be a point in the theoretical model for electric field strength calculation. A point-surface model is used to describe the electric field strength when the front end of the needle electrode is a plane of 300 μm radius in experiments. Figure 2f shows the distribution of normal forces acted on the abrasive particles within the polishing region under the same electric field intensity. The total force applied on abrasive

particles is determined by the electric field intensity and is the most important parameter for the ERFP process. Both of the forces F_{ep-ap} and F_{ap-ap} decrease rapidly away from the tool electrode center due to the quick decay of electric field intensity. It is also noted that the interaction force between the abrasive particles and starch particles is greater than that between the abrasive particles.

When an electric field is applied, the polarized ER particles form an array of stable chains along the field direction within the narrow working gap, where the abrasive particles attracted to the particle chain penetrate into the specimen surface by the exerted normal force. The material removal occurs as the indentation and shear movement of abrasive particles by a specific scratch manner between the abrasive particles and the specimen surface. The abrasive particles move in a certain polishing track relative to the specimen surface in the ERFP process, resulting in a regular removal area along a circular path (**Figure 3**).

When the penetrated abrasive particles are translated horizontally due to the shear force caused by the rotation of the sticky ER fluid, the workpiece surface will be polished with material removal. The indentation depth of the abrasive particles depends on the applied normal force and the material properties of specimen. The performance of specimen can be expressed by Brinell hardness when the spherical abrasive is pressed into the workpiece. Brinell hardness number H_{BHN} can be correlated with the depth of indentation into the workpiece as follows.[25]

$$H_{BHN} = \frac{2F}{\pi D_g (D_g - \sqrt{D_g^2 - D_i^2})} \tag{4}$$

where D_g is the diameter of the abrasive particle, $D_i = 2r_a$ as shown in Figure 3, and normal force F can be calculated by Equation (1). As shown in Figure 3, the depth t of indentation into the specimen can be expressed as

$$t = r_{ap} - (r_{ap}^2 - r_a^2)^{1/2} \tag{5}$$

Substituting Equation (5) into Equation (4), it can be obtained

$$t = \frac{F_n}{2\pi r_{ap} H_{BHN}} \tag{6}$$

The cross-sectional area A' (i.e., the shaded portion of the abrasive particle in Figure 3a) of the groove generated by the translation of the penetrated abrasive particle is derived by[26]

$$A' = r_{ap}^2 \arcsin\frac{\sqrt{t(2r_{ap} - t)}}{r_{ap}} - \sqrt{t(2r_{ap} - t)}(r_{ap} - t) \tag{7}$$

Considering $t \ll r_{ap}$, we can approximate $\sin\alpha \approx \alpha$. Thus, Equation (7) can be further simplified as

$$A' = t\sqrt{2tr_{ap}} \tag{8}$$

Substituting Equation (6) into Equation (8), we finally get the expression of cross-sectional area A'

$$A' = \frac{{F_n}^{3/2}}{2\pi^{3/2} r_{ap} {H_{BHN}}^{3/2}} \tag{9}$$

Thus, the total volumetric material removal is expressed as

$$V_t = \sum_{i=1}^{N} V_a^i N_i \tag{10}$$

where N_i is the number of the abrasive particles engaged in the material removal in the ith circular polishing path, V_a^i is the volume of material removed by an abrasive particle, N refers to the number of the circular polishing paths within the effective polishing area, r_0 is the radius of the effective polishing area, and r_i is the radius of the circular polishing path. Therefore, N_i can be calculated approximately by

$$N_i = 2m\pi r_i {N_0}^{1/2} \tag{11}$$

where $N_0 = \frac{3}{2}\frac{\varphi}{\pi r_{ep}^2}$ is the quantity of polymerizing chains located in a unit area, ϕ is the volume fraction of the ER particles, and V_a^i can be approximated by the cross-sectional area and the actual contact length. The actual contact length of the abrasive particle within the total finishing distance on the workpiece surface is as follows $v_i t$[27]

$$V_a^i = CA_i' \times v_i t \tag{12}$$

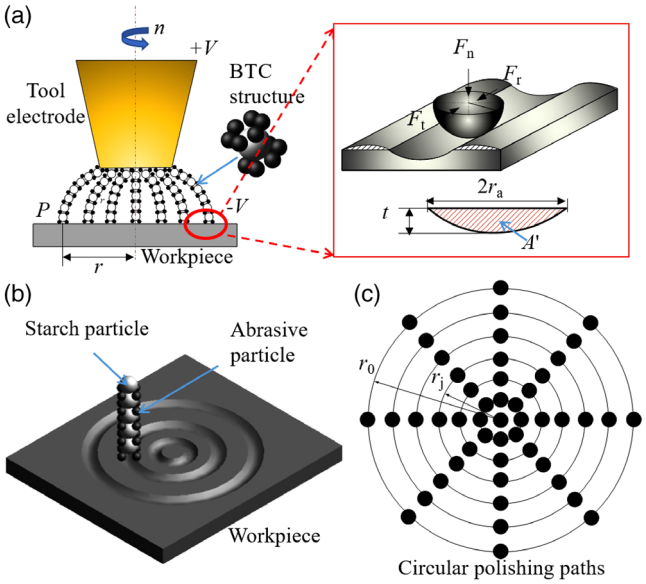

Figure 3. Material removal analysis in ERFP method for conductive materials. a) Schematic illustration of the removal mechanism for the conductor materials in ERFP. The tool electrode and specimen are connected with positive pole and negative pole, respectively. When an electric field is applied, the polarized solid particles form particle chains between the electrodes along the direction of the electric field. The abrasive particles are bonded on the surface of the polarized solid particles. The material removal occurs as the indentation and shear movement of abrasive particles by a specific scratch manner between abrasive particles and specimen surface. b) The tool electrode rotates to drive the particle chains running together, generating a circular removal path on the specimen surface. c) Schematic of the top view of the multiple circular polishing path in the polishing area formed by different particle chains.

where C is a coefficient related to material removal, v_i is the moving velocity of the abrasive particles in the ith circular grooving route, and t is the polishing time. Substituting Equation (9) into Equation (12), one can obtain

$$V_{\mathrm{a}}^{i} = \frac{C{F_{ni}}^{3/2} v_i t}{2\pi^{3/2} r_{\mathrm{ap}} {H_{\mathrm{BHN}}}^{3/2}} \tag{13}$$

Then, substituting Equation (11) and (13) into Equation (10), we can get

$$V_{\mathrm{t}} = \frac{6^{1/2}\mathrm{Cmt}\varphi^{1/2}}{2\pi r_{\mathrm{ep}} r_{\mathrm{ap}} {H_{\mathrm{BHN}}}^{3/2}} \sum_{i=1}^{N} {F_{ni}}^{3/2} v_i r_i \tag{14}$$

where $v_i = \omega r_i$, and ω is the angular velocity of ER polishing slurry.

When an electric field is applied, the ERFP fluid forms a rigid core attached with the rotating tool electrode. Thus, ω is calculated by the angular velocity ω_0 of tool electrode ($\omega_0 = 2\pi n$, where n is the spindle rotational speed of tool electrode).

$$V_{\mathrm{t}} = \frac{6^{1/2}\mathrm{Cmnt}\varphi^{1/2}}{r_{\mathrm{ep}} r_{\mathrm{ap}} {H_{\mathrm{BHN}}}^{3/2}} \sum_{i=1}^{N} {F_{ni}}^{3/2} r_i^2 \tag{15}$$

From Equation (14), the volumetric material removal of the ith circular polishing path can be derived as

$$V_{\mathrm{t}}^{i} = \frac{6^{1/2}\mathrm{Cmnt}\varphi^{1/2} {F_{ni}}^{3/2} r_i^2}{r_{\mathrm{ep}} r_{\mathrm{ap}} {H_{\mathrm{BHN}}}^{3/2}} \tag{16}$$

The volumetric material removal of the jth circular polishing path within the effective polishing area can be approximated by

$$V_{\mathrm{t}}^{i} = 2\pi W h_i r_i \tag{17}$$

where W is the width of material removal in the jth circular polishing path, and h is the depth of material removal obtained in the jth circular polishing path after polishing of N times. W is equal to $2R_{\mathrm{w}}$, as shown in Figure 3, and Equation (17) can be rewritten as

$$V_t^{i} = 4\pi R_w h_i r_i \tag{18}$$

where R_0 can be calculated by $R_{\mathrm{w}} = [(r_{\mathrm{ep}} + r_{\mathrm{ap}})^2 - ({r_{\mathrm{ep}+\delta/2}}^2)^2]^{1/2}$. Substituting Equation (18) into Equation (18) yields

$$h_i = \frac{6^{1/2}\mathrm{Cmnt}\varphi^{1/2} {F_{ni}}^{3/2} r_i}{4\pi r_{\mathrm{ep}} r_{\mathrm{ap}} [(r_{\mathrm{ep}} + r_{\mathrm{ap}})^2 - (r_{\mathrm{ep}} + \delta/2)^2] {H_{\mathrm{BHN}}}^{3/2}} \tag{19}$$

where F_{ni} can be calculated by Equation (1), and h_i is a function of r_i. The material removal profile along the radial direction within the polishing area, calculated by Equation (19), is comprised of the material removal depths caused by the different single circular polishing paths.

The material removal experiments of conductive materials are performed using a five-axis ER fluid-assisted polishing equipment with tunable working gap and rotation speed. The microstructure, removal depth, and polishing region are measured by a Wyko NT1100 interferometer. The experimental parameters are summarized in **Table 1**. **Figure 4**a presents the material removal profile along the radial direction within the polishing region by the theoretical calculation and the experimental measurements under the same conditions (i.e., 5 V, 50 μm, and 1000 rpm). The simulated material removal profile agrees very well with the measured results, which confirms that the proposed model is valid to predict the material removal profile along the radial direction within the polishing region in the ERFP process for conductive materials.

Table 1. Experimenting parameters.

Control parameters	Values
Supply voltage	5 V
Rotational speed	100–3000 rpm
Working gap	20–60 μm
Radius of tool tip	0.3 mm
Starch particle size	10 μm
Diamond particle size	5 μm
Volume percentage of starch particle	30%
Volume percentage of abrasive particles	10 wt%
Abrasive	Diamond
Workpiece	Tungsten carbide
Brinell hardness number of tungsten carbide	810 MPa

Figure 4b shows the microstructure of the polished specimen surface and material removal profiles within the polishing region at the central region and along the radial direction, respectively. Ring-shaped grooves caused by abrasive particles appear within material removal region in the ERFP process. The radius of the polishing region is around 300 μm, and the shape of the measured material removal profile looks like a "W." The maximum depth of material removal is about 12 μm and located at 120 μm far from the center of the polishing region. It is observed that the volume of material removal at the center of the polishing region is less than that in the surrounding areas due to the lower shear velocity of ER slurry in the center part. The electrical field strength and the normal force gradually decrease along the radial direction within polishing region. Although the velocity of ER polishing slurry increases at the edge of the sample, the volume of slurry decreases remarkably toward the edge of the polishing region, making the material removal rate decreases significantly due to the increasing amount of escaping abrasive particles from polishing region. The size of the tool electrode is an important factor for material removal in ERFP. The size of the front end of the tool electrode affects the electric field distribution in the polishing area; i.e., a smaller front end generates a weaker electric field in the polishing center area. The decrease of the normal force acting on the abrasive particles due to the weak electric field then results in a low material removal rate in the center region of the polishing area. Therefore, the height of the hump of the material removal profile "W" will increase with a small and delicate tool electrode, and the abrasive particles are aggregated in front of the electrode, resulting in a finer polishing profile. On the contrary, if a larger size of tool electrode is utilized, the centrifugal force will become larger and make abrasive particles difficult to gather in the front of tool electrode.

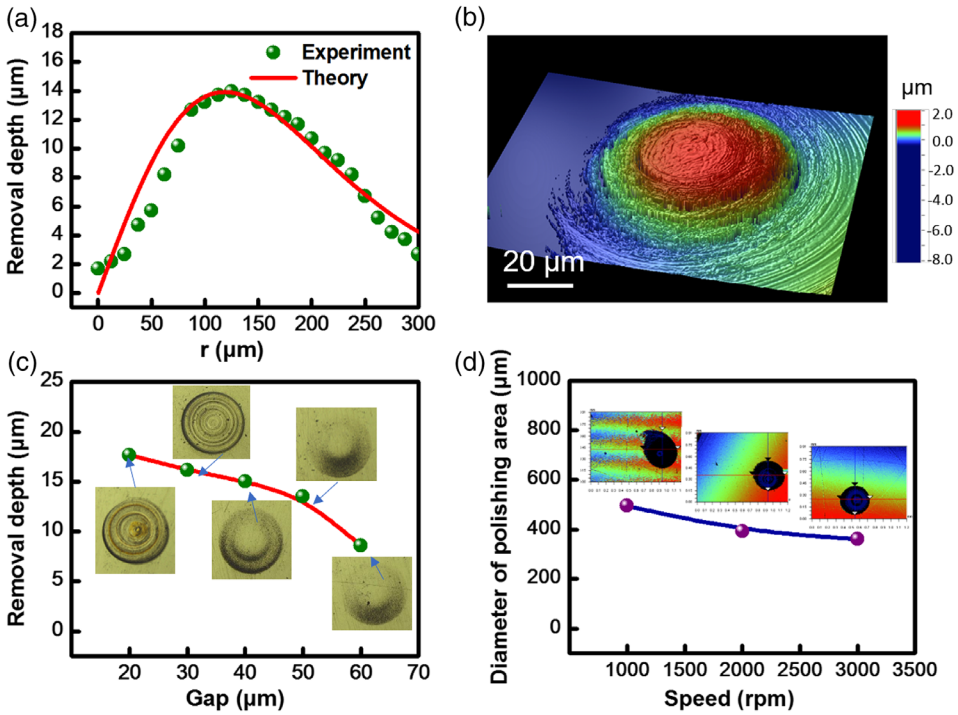

Figure 4. Experiment measurement and analysis for polishing tungsten carbide. a) The material removal profile obtained by experimental measurements and proposed removal model with a coefficient C of 1.6×10^9. b) 3D material removal profile of the polished surface with diamond abrasive particles, measured by a profilometer. c) The maximum removal depth of ERFP as a function of gap size. d) The effect of the rotation speed of tool electrode on the effective polishing area in ERFP.

Figure 4c shows the relationship between the maximum removal depth and the gap size. The removal depth decreases dramatically with the increasing gap size, indicating that the gap size is a key parameter of the polishing process. When the gap is ≈20 μm, the ER polishing slurry is discharged for a short time, leading to the tool electrode residue in the polishing area. Figure 4d demonstrates the effect of rotation speed of a tool electrode on the effective polishing area of a workpiece surface. The electric field strength decreases with the distance away from the polishing center, resulting in a lower bonding ability of ER particles in the particle chains with abrasive particles. Moreover, the abrasive particles cannot participate in polishing effectively due to the increase of the centrifugal force. Therefore, the range of effective removal region decreases with the increase in tool electrode speed.

In summary, we have investigated the feasibility and performance of the ERFP process in polishing the surfaces of conductive materials. A theoretical model for the material removal volume is derived for ERFP to predict the polishing performance and the final profile of a workpiece. The microstructure models for different size ratios of the particles in ERFP slurry are discussed. The normal forces on the abrasive particles from the applied electric field and the material removal process are analyzed. Material removal volume decreases gradually along the radial direction from the center of polishing region. The measured material removal profile agrees well with the theoretical prediction, confirming the validity of the proposed model. The removal volume rapidly decreases with the increase in the gap size and the rotation speed, which leads to the reduction of electric field strength and the increasing of the centrifugal force. The material removal depth varies dramatically from less than 9–18 μm when the gap is in 10–60 μm under an applied voltage of 5 V, and the diameter of polishing area changes from 375 to 572 μm with a rotation speed ranging from 1000 to 3000 rpm. Experiments show that with Tungsten carbide abrasive particles under various gap sizes and rotation speeds, a maximum material removal depth of 18 μm and a minimum polishing diameter of 375 μm can be obtained, demonstrating the ability of polishing conductive materials with high resolution and accuracy, such as a microneedle-like tool electrode.

Supporting Information

Supporting Information is available from the Wiley Online Library or from the author.

Acknowledgements

Y.Z. and X.L. thank the financial support from the Science and Technology Development Project of Jilin, China (JJKH20156413). C.C. acknowledges the support of the startup grant from Michigan State University.

Conflict of Interest

The authors declare no conflict of interest.

Keywords

conductive materials, electrorheological fluids, material removal, polishing, ultra-precision processing

Received: September 16, 2020
Revised: October 23, 2020
Published online:

[1] W. K. Chen, T. Kuriyagawa, H. Huang, N. Yosihara, *Precis. Eng.* **2005**, *29*, 315.
[2] T. Kaku, T. Kuriyagawa, N. Yoshihara, *Int. J. Manuf. Technol. Manage.* **2006**, *9*, 109.
[3] S. Yin, T. Shinmura, *Int. J. Mach. Tools Manuf.* **2004**, *44*, 383.
[4] H.-y. Tam, H. Cheng, *J. Mater. Process. Technol.* **2010**, *210*, 807.
[5] T. C. Halsey, *Science* **1992**, *258*, 761.
[6] T. Hao, *Adv. Colloid Interface Sci.* **2002**, *97*, 1.
[7] T. Do, H. Lee, Y. G. Ko, Y. Chun, U. S. Choi, C. H. Kim, *Colloids Surfaces A, Phys. Eng. Aspects* **2017**, *514*, 56.
[8] M. H. Kim, D. H. Bae, H. J. Choi, Y. Seo, *Polymer* **2017**, *119*, 40.
[9] A. Egorysheva, V. A. S. Kraev, O. M. Gajtko, T. Kusova, V. A. E. Baranchikov, A. Agafonov, V. V. K. Ivanov, *Powder Technol.* **2020**, *360*, 96.
[10] J. Noh, C. M. Yoon, J. Jang, *J. Colloid Interface Sci.* **2016**, *470*, 237.
[11] H. Wu, Z. C. Xu, J. B. Wu, W. J. Wen, *Int. J. Modern Phys. B* **2018**, *32*, 1.
[12] Y. Z. Dong, Y. Seo, H. J. Choi, *Soft Matter* **2019**, *15*, 3473.
[13] C. M. Vu, V.-H. Nguyen, Q.-V. Bach, *J. Mol. Liquids* **2020**, *314*, 113762.
[14] S. Zhang, W. T. Winter, A. J. Stipanovic, *Cellulose* **2005**, *12*, 135.
[15] T. Kuriyagawa, M. Saeki, K. Syoji, *Precis. Eng.* **2002**, *26*, 370.
[16] W. B. Kim, S. J. Lee, Y. J. Kim, E. S. Lee, *Int. J. Mach. Tools Manuf.* **2003**, *43*, 81.
[17] L. Zhang, X.-S. He, H.-R. Yang, Y. Zhang, *Int. J. Mach. Tools Manuf.* **2010**, *50*, 737.
[18] L. Zhang, T. Kuriyagawa, T. Kaku, J. Zhao, *Int. J. Mach. Tools Manuf.* **2005**, *45*, 1461.
[19] Y. Akagami, N. Umehara, *Wear* **2006**, *260*, 345.
[20] J. Su, H. Cheng, Y. Feng, H. Y. Tam, *Appl. Opt.* **2016**, *55*, 638.
[21] L. Zhang, Y.-W. Zhao, X.-S. He, T. Kuriyagawa, *Int. J. Mach. Tools Manuf.* **2008**, *48*, 295.
[22] J. S. Su, H. B. Cheng, Y. F. Wen, Y. P. Feng, H. Y. Tam, *J. Mater. Process. Technology* **2016**, *238*, 124.
[23] J. B. Lu, Q. S. Yan, H. Tian, L. Y. Kong, *J. Mater. Process. Technol.* **2009**, *209*, 4954.
[24] Y. Y. Tsai, C. H. Tseng, C. K. Chang, *J. Mater. Process. Technol.* **2008**, *201*, 565.
[25] S. Jha, V. K. Jain, *Wear* **2006**, *261*, 856.
[26] M. Das, V. K. Jain, P. S. Ghoshdastidar, *Int. J. Mach. Tools Manuf.* **2008**, *48*, 415.
[27] J. D. Kim, M. S. Choi, *J. Mater. Process. Technol.* **1995**, *53*, 630.

